Measurements of Soot Production and Thermal Radiation From Confined Turbulent Jet Diffusion Flames of Methane

S. J. BROOKES[1] and J. B. MOSS*

School of Mechanical Engineering, Cranfield University, Bedford MK43 0AL England

Turbulent methane/air jet diffusion flames at atmospheric and elevated pressure have been studied experimentally to provide data for coupled thermal radiation and soot production model development and validation. Although methane is only lightly sooting at atmospheric pressure, at elevated pressure the soot yield increases greatly. This allows the creation of a highly radiating flame, of moderate optical depth, within a laboratory scale rig. Spatially resolved flame properties needed for model validation have been measured at 1 and 3 atm. These measurements include detailed maps of mean mixture fraction, mean temperature, mean soot volume fraction, and mean and instantaneous spectrally resolved, path integrated radiation intensity. © 1998 by The Combustion Institute

NOMENCLATURE

Latin

AFR	Air to fuel mass ratio
f_V	Soot volume fraction
I	Intensity—(W m^{-2} sr^{-1})
k	Imaginary component of the refractive index
m	Complex refractive index
n	Real component of the refractive index
N	Soot particle number density—(m^{-3})
Q	Efficiency factor
r	Radial position/soot particle radius—(m)
x	Spatial coordinate—(m)

Greek

α	Size parameter
κ	Absorption coefficient—(m^{-1})
λ	Wavelength—(m)
ξ	Mixture fraction

Subscripts

0	Initial value
λ	At wavelength λ
Abs.	Absorption
Ext.	Extinction
Max.	Maximum value

*Corresponding author.

[1]Present Address: Engineering Department, University of Cambridge, Trumpington Street, Cambridge, CB2 1PZ England.

INTRODUCTION

Two of the principal hazards from an accidental fire arise from the thermal radiation, which is mainly emitted from soot particles within the flame, and from the liberated smoke, which may include product gases, carbon particulates, and condensed hydrocarbon droplets. Thermal radiation is a major factor in determining the rate of fire spread and in causing damage to surrounding structures, while the smoke restricts visibility and impedes evacuation.

Computational models for the prediction of flame behavior have obvious advantages over bespoke experimental studies, particularly in respect of hazard assessment. However, while the calculation of general turbulent flame structure is now arguably within the capabilities of computational fluid dynamics (CFD), the additional problems of soot production and flame radiation are not adequately resolved for confident prediction.

Large quantities of soot may be produced within diffusion flames the soot forming as a result of fuel pyrolysis in the high temperature, fuel rich regions. The processes of soot formation and oxidation are highly temperature dependent and soot is usually the dominant radiating species in hydrocarbon fuelled flames. Therefore, an intimate coupling exists between soot production and radiative heat transfer from the flame. However, despite this coupling it has been customary in modelling studies to decouple these effects, either by prescribing the degree of heat loss, determining the soot prop-

COMBUSTION AND FLAME 116:49–61 (1999)

Published by Elsevier Science Inc.

0010-2180/99/$19.00
PII S0010-2180(98)00027-3

erties from non-coupled balance equations or by prescribing the soot concentration and post-processing the computation of the radiative flux [1–4]. The aim of the present work is to provide a sound experimental background against which to develop a more comprehensive prediction of the levels of soot and radiation from turbulent jet diffusion flames.

Methane has been selected as the fuel for this study because it occupies (as natural gas) a central position in the energy field, in relation to both utilization and to transmission and storage. Additionally, the chemistry of methane combustion is comparatively well known. No extensive soot measurements have been reported in turbulent methane flames to date, however, due to the difficulty in measuring the low levels of soot found in laboratory scale flames burning at atmospheric pressure. At large scale, methane fires soot quite heavily due to the increased time scales under high temperature, fuel rich conditions. However, measurements at such scales, in both pool fires and jet flames, have tended to focus on global properties and provide limited information with the resolution required for model development. This work seeks to emulate a larger scale methane jet flame in the laboratory by operating the flame at elevated pressure. At 3 atm the peak soot concentration is increased by a factor of approximately 10 and the heat loss from the flame is approximately doubled, when compared to a flame of the same fuel mass flow operating at atmospheric pressure.

Open turbulent jet flames fuelled by methane have been studied quite extensively [5, 6] but typically with a view to capitalizing on the reduced radiative heat loss accompanying the low levels of particulate soot generated. The present investigation has the objective of creating the database of soot and related properties in a confined jet flame, necessary to develop and evaluate a generally applicable methodology for coupled radiation and soot prediction in turbulent hydrocarbon flames.

RIG GEOMETRY AND BURNER DESIGN

During the course of this experimental study two rigs have been employed, although the boundary conditions presented to a flame by these two rigs are almost identical. The first rig was designed for studying turbulent jet flames at both atmospheric and elevated pressure. The body of the rig forms a cylindrical pressure vessel and consists of five main stainless steel sections (see Fig. 1). The bottom section is made from a blank flange, through the center of which passes a shaft carrying the burner. The gases for the main fuel flow and the premixed pilot pass through this shaft, while holes drilled in the flange admit the air for the co-flow. Bolted to this flange, forming the main body of the rig, are two sections of pipe. Between these is the measurement section, machined from a single billet of stainless steel. Four windows may be mounted in this section, allowing optical access to 75 mm of the flame width. Two window types are utilized. Circular quartz windows, giving good optical access to the flame, are generally used. However, for the radiation intensity measurements, quartz is not a suitable optical material as it absorbs strongly at wavelengths longer than ~2.5 μm. For the radiation intensity measurements the quartz windows

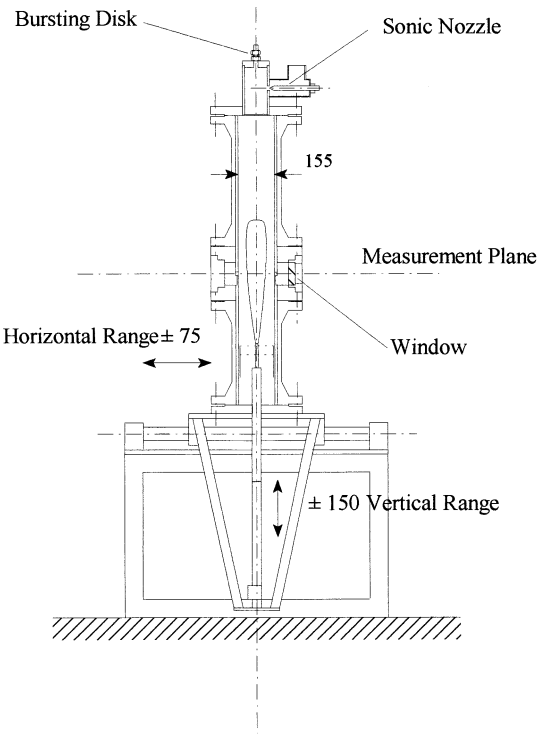

Fig. 1. Elevated pressure rig. All dimensions in mm.

were therefore replaced by sapphire slot windows, having the same width as the quartz windows but with a viewable area of only 10 mm in height. Provision has also been made for probes to be mounted on the measurement section, which may be traversed across the full width of the flame. At the top of the rig, closing the vessel, is a bursting disk and choked-nozzle pressurising valve assembly. The burner has a vertical movement range of 300 mm and, coupled with the use of unequal length main tube sections, which may be interchanged, allows 425 mm of the flame height (measured from the burner exit plane) to be investigated. The flame is contained by a Pyrex tube of internal diameter of 155 mm mounted inside the vessel. In order to allow unobstructed optical and probe access to the flame, the Pyrex tube is split into two sections separated by a slotted stainless steel spacer ring, which is 8 mm in height. The entire pressure rig is mounted on a movable platform which may be traversed horizontally (perpendicular to the flame axis) over a range of approximately 150 mm. This allows the flame to be traversed using fixed optical systems on either side of the rig.

The second rig was designed for operation at atmospheric pressure alone but provided some additional operational flexibility. The rig is essentially the same as that previously described but does not include the external pressure vessel. The flame is again confined in a Pyrex tube of internal diameter 155 mm, split at approximately the mid-point, and separated by a stainless steel spacer. However, in this case the spacer ring itself is machined to directly accept sapphire slot windows. The only data reported here from this rig are the 1 atm radiation intensity measurements. Measurements of temperature and soot volume fraction were taken in each rig, for the same (1 atm) flame conditions. The measured data from each rig were identical (within the bounds of experimental uncertainty), confirming that the pressure casing and associated valve assembly did not distort the flame in the region where measurements were taken.

To avoid the complication of modelling a lifted flame with the associated uncertainties in the upstream boundary condition, it is very important that the flame be stabilized at the exit

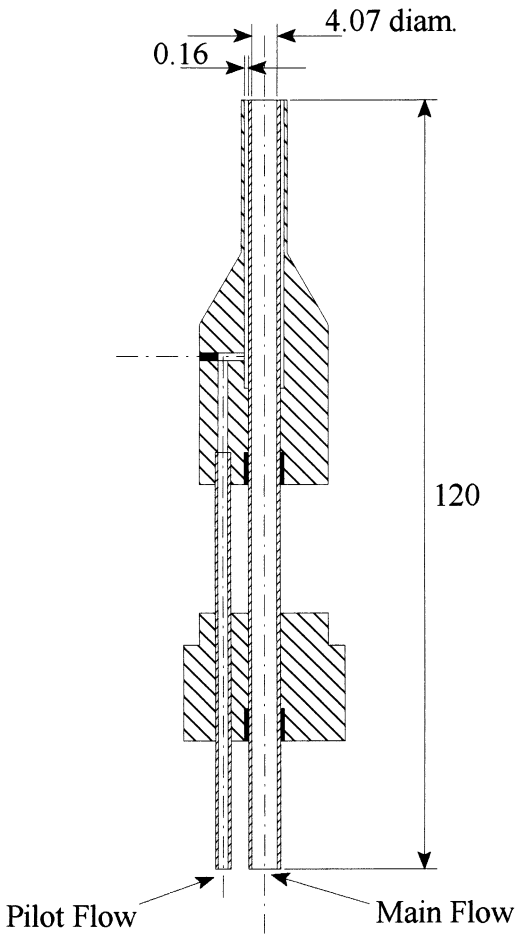

Fig. 2. Piloted methane burner. All dimensions in mm.

of the burner. A cylindrical nozzle was therefore constructed with an annular premixed pilot flame, of 160 μm width, surrounding the main fuel jet. A 4.07 mm diameter orifice for the main fuel flow was found to give a reasonable compromise between flame size and flame stability. However, even with an annular pilot flame, the jet flame is stable only to an exit Reynolds number of 5000, at atmospheric pressure. The detailed burner design is shown in Fig. 2. Attention has been paid to the aerodynamics of the sensitive near-burner region in an attempt to avoid recirculation around the base of the flame caused by the air co-flow. Mounted on the burner, below the level of the burner tip, is a flow-straightening diffuser, consisting of two circular, perforated metal plates the function of which is to flatten the velocity profile in the co-flowing air. The operating conditions for the

TABLE 1

Operating Conditions for the Flames Investigated

Absolute pressure/atm	1 (Flame 1) and 3 (Flame 2)
Fuel mass flow/g min^{-1}	10.3
Air mass flow/g min^{-1}	708
Fuel temperature/K	290
Air temperature/K	290
Fuel jet velocity/m s^{-1}	20.3 (Flame 1) and 6.77 (Flame 2)
Exit Reynolds number	5000

two flames investigated in this study are summarised in Table 1.

The pilot flame is a premixture of methane and oxygen, having a methane flowrate <2% of the main fuel flowrate. This pilot flame is burnt fuel rich to prevent overheating of the burner tip. At 3 atm the pilot flame shows a tendency to burn back to the premixing point, which may be prevented by careful tuning of the ratio of O_2 to CH_4. Flame 1 displays a visible flame height of around 600 mm, viewed with the external pressure vessel removed. Visual access to Flame 2 is limited by the pressure vessel, but this flame appears to be smaller, with a height of approximately 400 mm.

MEAN MIXTURE FRACTION MEASUREMENT

Two methods were used for mean mixture fraction measurements in the turbulent flame, each relying on a probe to draw gas samples from the flame. The technique employed most extensively here infers the mixture fraction from the measurement of local carbon to nitrogen ratio. A sample of gas is continuously drawn from the flame through a quartz probe, which has an outside diameter of approximately 6 mm, tapering to a tip with an orifice internal diameter of approximately 500 μm. Oxygen, flowing through a ceramic tube running along the center of the probe, is mixed with the incoming sample gas near to the probe entrance. This mixture, of sample gas and oxygen, passes along the length of the probe over an electrically heated platinum catalyst. Young [7] gives full details of the probe design. In the presence of excess oxygen and the catalyst all of the carbon bearing species oxidise to CO_2 and H_2O. This gives a product gas comprising CO_2, H_2O, O_2, and N_2 alone, which is passed to a calibrated mass spectrometer for determination of the mole ratio of carbon dioxide to nitrogen. The mixture fraction (ξ) is then obtained from

$$\xi = \frac{1}{1 + AFR}, \tag{1}$$

where the air-fuel ratio (AFR) is given by

$$AFR = \frac{[N_2]}{[CO_2]} \frac{28 + (0.21/0.79) \times 32}{16} \tag{2}$$

and $[N_2]/[CO_2]$ is the measured mole ratio of nitrogen to carbon dioxide. Problems were encountered in the high mixture fraction regions near the burner exit ($\xi > 0.4$). Under these conditions the reaction between the oxygen and the sample gas, with its associated volumetric expansion, can lead to flow reversal with oxygen leaving the tip of the probe. The measurements were therefore confined to regions in the flame with a mixture fraction below 0.4, from approximately 150 mm downstream of the burner exit in the 1 atm flame. Upstream of this 0.4 mixture fraction limit, the mixture fraction was measured more directly, by mixing a tracer species with the methane fuel. The tracer used was argon, mixed to give a fuel gas stream consisting of 90% methane and 10% argon by volume. The gas sample drawn through the quartz probe is passed directly to the mass spectrometer and the AFR, inferred from the ratio of argon to nitrogen, is determined using the relationship

$$AFR = \frac{[N_2]}{[Ar]} \frac{28 + 0.21/0.79 \times 32}{1 \times 40 + 9 \times 16} \tag{3}$$

Only three data points in the data set were obtained using this technique, those at 50, 100, and 150 mm above the burner exit plane on the flame axis.

The repeatability of the measurements was generally good. An estimate of the absolute uncertainty was obtained by measuring the carbon dioxide to nitrogen ratio of a gas mixture with an accurately known composition. The effective measured mixture fraction of this gas may then be calculated and compared with the calibration value. The calculated mean error was 6% and is of the same order as the repeat-

ability of the measurement. However, the mean mixture fraction does not fall to zero at the edges of the flame, as would be expected. Examination of Eqs. 1 and 2 reveals that for the mixture fraction to reach zero the *AFR* must be infinity and the concentration of carbon dioxide must fall to zero. In practice there is always a small background level of carbon dioxide present in the mass spectrometer, most probably absorbed in water deposited on the inside of the sample line; therefore a mixture fraction measurement of zero is not attainable. The minimum mixture fraction measured, corresponding to this background level of carbon dioxide, is approximately 0.02.

MEAN TEMPERATURE MEASUREMENT

Mean temperature was measured with a fine wire thermocouple of 50 μm diameter Pt and Pt 87%/Rh 13% wires (Type R). These wires were flame welded to form a junction bead of <200 μm diameter. The thermocouple junction was mounted on support wires, made from the same combination of materials, of 500 μm diameter. These passed through a dual bore ceramic tube, which was mounted in a stainless steel probe body. At one end of the ceramic tube the support wires were connected to a standard R type thermocouple connector; at the other, the wires were bent outwards in the form of a "V." The support wires extended approximately 30 mm beyond the end of the ceramic tube and the widest end of the "V" was approximately 20 mm across. It was at the wide end of the "V" that the thermocouple junction was mounted. The thermocouple voltage was measured with a 12-bit resolution analogue-to-digital conversion system mounted in an IBM compatible computer. The temperature samples were taken at 1 kHz; 5000 samples were found to give a stationary mean temperature at any given flame location. The mean temperature values have been corrected for radiative loss from the bead of the thermocouple using the method described by Fristrom and Westenberg [8]. No visible soot deposition on the thermocouple was apparent in either the 1 or 3 atm methane flame; hence, the bead emissivity was taken to be that for bright Platinum at 1500 K, with a value of $\sim$0.2. With a typical bead diameter of 150 μm the maximum correction applied to the temperature data was approximately 50 K. It was not possible to compensate for the effect of conduction along the bead support wires, due to the uncertain time-varying temperature field in the turbulent flames. As the study considers diffusion flames, and the combustion is mixing controlled, catalytic effects have also been neglected. The temperature measurements demonstrate excellent repeatability.

MEAN SOOT VOLUME FRACTION MEASUREMENT

Laser extinction tomography was used to measure mean soot volume fraction in the turbulent methane flames under study. The technique relies on a mathematical inversion of path-integrated extinction data to give the extinction coefficient, and hence the soot volume fraction, as a function of position. The mean extinction profile, in the form of the intensity ratio $\overline{\ln\,(I(x)/I_o)}$ may be inverted in three different ways to give the mean extinction coefficient as a function of radial position in the flame, $\overline{\kappa(r)}$. The three principal reconstruction methods are "onion peeling," Abel transformation, and Fourier convolution. Hughey and Santavicca [9] outline these techniques and compare them in terms of their ability to reconstruct reacting and non-reacting flowfields from simulated absorption data. They conclude that each reconstruction process can yield "artifacts," which are not actually present in the flowfields, and recommend the use of more than one of these methods to distinguish real features from those which are artifacts of the reconstruction. Two reconstruction methods have been used in this work; "onion peeling" and Fourier convolution.

The "onion peeling" technique divides the flow field into n concentric rings, within which the soot is considered to be homogeneously distributed, where n is the number of absorption measurements taken. A disadvantage of this method is that, as the extinction coefficient is solved for sequential rings from the outside inwards, errors tend to build up to a maximum at the center of the flowfield. Full derivation of the Fourier convolution method is given by

Shepp and Logan [10]. It suffers from the disadvantages that the reconstruction at discontinuities in $\overline{\kappa(r)}$ may produce oscillating overshoots. Following [7], the experimental data are smoothed by fitting a high-order polynomial before reconstruction. Using the smoothed experimental absorption datasets, no difference was found between the results of the two reconstruction algorithms used.

The extinction of electromagnetic radiation by soot particles is related to the size of the particles, their refractive index, the wavelength of the incident radiation, and the number density of the particles. For spherical particles the extinction coefficient may be written as

$$\kappa_{\text{Ext.},\,\lambda} = \int_0^\infty N(r)\,\pi r^2 Q_{\text{Ext.}}(\lambda, m, r)\,\mathrm{d}r, \tag{4}$$

where r is the particle radius. The extinction of the radiation includes contributions from both absorption and scattering. If the soot particles are small in comparison to the wavelength of the radiation ($2\pi r/\lambda \ll 1$), the Rayleigh limit, the component arising from the scattering of the radiation is negligible in comparison with the absorption: $Q_{\text{Ext.}} \simeq Q_{\text{Abs.}}$. If, in addition, the soot particles are assumed to be spherical then the absorption efficiency is given by the Lorentz-Mie theory [11] as

$$Q_{\text{Abs.}} = \frac{48\pi nkr}{\lambda[4n^2k^2 + (n^2 - k^2 + 2)^2]}. \tag{5}$$

This may be substituted into Eq. 4 to give the absorption coefficient for soot in the Rayleigh limit

$$\kappa_{\text{Abs.},\,\lambda} = \frac{36\pi nk}{\lambda[4n^2k^2 + (n^2 - k^2 + 2)^2} \cdot \int_0^\infty N(r)\,\frac{4}{3}\,\pi r^3\,\mathrm{d}r, \tag{6}$$

where the integral is simply the volume fraction, f_{V}, of the soot particles.

The 5 mW Helium-Neon laser operated at 632.8 nm. The value of the complex refractive index adopted is that proposed by Mullins and Williams [12] for propane soot at this wavelength, with a value of $m = 1.92 - 0.45\,i$. This particular refractive index value was simply chosen to maintain continuity with previous work at Cranfield [3, 13]. The soot particles may be expected to reach a maximum diameter of 30 nm in the 1 atm flame, based on laminar flame measurements [14]. In the 3 atm flame, where the measured mean absorption is an order of magnitude greater, this maximum particle diameter may be expected to reach 60 nm. Hence, the Rayleigh condition is certainly satisfied in the 1 atm flame but in the 3 atm flame some inaccuracy may be expected because of the larger particle size. The repeatability of the measurement was good in the regions of the flame where the soot volume fraction was high ($>$0.5 ppm).

Uncertainties in the measured soot volume fraction have four principal sources; these are errors in the measurement of the mean extinction profile, in the value of the refractive index chosen, in the application of the Rayleigh limit, and in the assumption that the particles are spherical.

The principal source of uncertainty in the extinction profile measurement is that arising from fluctuations in laser power, given the weakly sooting nature of the fuel and consequently small laser absorption. Extinction profiles in the 1 atm flame were recorded at 300, 350, and 425 mm above the burner exit plane. The highest mean absorption measured is encountered at the 425 mm height, but even here the peak value is only 5%. A typical 1% variation in the power output of the laser, therefore, would give an error of 20% in the measured signal. At 3 atm the peak absorption measured is approximately 20% at 250 mm from the burner exit plane. A similar laser power fluctuation would give only a 5% error at this height. Clearly, these errors in the extinction profile represent minimum values near the centre of the profile, where the absorption is at its highest.

Recasting Eq. 6 in the form

$$f_{\text{V}} = f(m)\lambda\kappa_{\text{Abs.}\lambda} \tag{7}$$

identifies $f(m)$, where

$$f(m) = \frac{4n^2k^2 + (n^2 - k^2 + 2)^2}{36\pi nk}. \tag{8}$$

TABLE 2

Representative Values for the Complex Refractive Index of Soot From the Literature

Author	Fuel	m	λ/nm	$f(m)$
Dalzell and	Propane	1.56–0.52i	650	0.228
Sarofim [15]	Acetylene	1.57–0.44i		0.256
Lee and Tien [16]	Iso-octane	1.9–0.55i	632.8	0.275
	Polystyrene			
	Plexiglass			
Mullins and Williams [12]	Methane	1.93–0.39i	632.8	0.391
	Propane	1.92–0.45i		0.338
	n-Heptane	1.89–0.44i		0.337
	Toluene	1.89–0.46i		0.323
Chippet and Gray [17]	Propane	1.9–0.35i	Visible	0.420

A range of values have been proposed for the complex refractive index of soot, $m = n - ki$ (Table 2).

Widely employed values give $f(m)$ varying by approximately a factor of 2. If it is assumed that the actual value for the soot lies somewhere in this range then the value of m used here ($m = 1.92 - 0.45i$) may introduce an error of up to $\pm 30\%$.

The Rayleigh limit analysis assumes $\alpha = 2\pi r/\lambda \ll 1$. Selamet and Arpaci [18] plot the percentage error using the Rayleigh limit instead of the exact solution for values of the size parameter α. In the 1 atm flame, where the soot particles may be expected to reach 30 nm diameter, the value of the size parameter is 0.15. In the 3 atm flame, where the soot particles may be up to 60 nm in diameter, the value of α is 0.3. These values of α yield errors of approximately 5% and 10%, respectively.

Thermophoretic sampling of soot and subsequent examination by transmission electron microscopy has shown that the soot in diffusion flames is a chain-like agglomeration of near spherical primary particles of ~40 nm diameter, with an average number of these particles per agglomerate of 34 [19]. Numerical simulations of agglomerate scattering and extinction by Kumar and Tien [20] indicate that for random clusters of primary particles numbering less than 40 the extinction of the agglomerate differs little from that of the same number of separate primary particles.

Summing the errors from each of the four principal sources reveals that the mean soot measurement may be subject to an overall error of approximately $\pm 50\%$ in both of the flames studied. The error is similar for each of the flames despite the relatively high soot loadings of the 3 atm flame. This is due to the increasing importance of light scattering from the larger soot particles formed in the 3 atm flame which cancels out any increase in the signal to noise ratio encountered due to the higher soot levels at 3 atm.

RADIATION INTENSITY MEASUREMENT

Mean and instantaneous spectrally resolved radiation intensity measurements were made in both the 1 atm and the 3 atm turbulent methane flames using a range of scanning monochromators (Rees Instruments, Codalming, England). The monochromators, which are small enough to be mounted on an optical rail, comprise a spectrometer, which contains a motor driven, constantly spinning diffraction grating (at 12 Hz), and a detector unit. The time taken for a scan across the full wavelength range of the monochromator is 42 ms. Two separate detector/grating combinations were employed; a germanium detector covering the range 600–1900 nm and an overlapping cooled lead selenide detector for the range 1500–5000 nm. Second order blocking filters in conjunction with the two detector units prevented lower wavelength spectral details appearing at positions in the spectra at twice their original wavelengths. Two filters were used with the germanium detector, covering the ranges 600–1100 nm and 1100–1900 nm. Three filters were used with the lead

selenide detector, covering the ranges 1500–2000 nm, 1650–3000 nm, and 2450–5000 nm. A simple optical arrangement, consisting of a Ca Fl_2 lens, an aperture and the monochromator slit (0.89 mm), defined the ray collected by the monochromators. Each instantaneous measurement recorded by the spectrometer/computer system is a path integral of the properties along the ray. The ray itself is almost rectangular in cross section, having a major dimension aligned parallel to the axis of the flame, which varied across its width, from approximately 5 mm on the side of the flame nearest to the monochromator to approximately 10 mm on the far side. The corresponding minor cross sectional dimension increased from approximately 2 mm to approximately 5 mm. The complete system was calibrated against a standard electrically heated blackbody furnace.

The measurements were made on optical paths that passed perpendicularly through the axis of the flames. Two mean intensity measurements were taken at each vertical measurement station with each grating/detector filter combination. Each mean measurement was determined from 500 samples. These two datasets were compared to check the repeatability of the measurement and then averaged to give a final mean of 1000 samples. The individual mean spectra from each grating/detector/filter combination are joined in the regions of overlap. The measurements in the 1500–2000 nm region were found to be redundant and therefore not used. The other four measurement sets (600–1100, 1100–1900, 1650–3000, 2450–5000 nm) were joined at 1100, 1750, and 2750 nm. At these points the spectra were found to overlap/join perfectly. The spectra recorded in the 3 atm flame exhibit a strong absorption "hole" in the 4300 nm CO_2 band which did not disappear after calibration. This is believed to originate with the rig configuration in which the measurements were made. The radiation measurements in the 1 atm flame employed the atmospheric flame rig, while those at 3 atm were made with the flame confined in the pressure casing. An undesirable feature for the elevated pressure rig is the existence of a nearly stagnant region of gas between the inner Pyrex flame tube and the rig windows in the external casing. It is likely that combustion products fill this space and the relatively cool CO_2 present in the combustion products then absorbs some of the flame radiation.

Instantaneous, "single-shot" spectra were also recorded at a single height of 250 mm in both flames. The optical path of the spectrometer again passed perpendicularly through the axis of the flames. Because the time taken for a single spectral scan is 42 ms the wavelength points in each spectra are not in general correlated. However, from these "single-shot" spectra, radiation statistics at specific wavelengths may be determined. For each flame approximately 150 "single-shot" spectra were recorded using two of the grating/detector filter combinations. The two grating/detector/filter combinations cover the ranges 1100–1900 nm and 2450–5000 nm. For each set of spectra, four wavelength points were chosen at which the intensity statistics were calculated. For the 1 atm flame these points were 1650, 2834, 3332, and 4359 nm. For the 3 atm flame these points were 1700, 2846, 3342, and 4435 nm. These points were chosen to represent the peaks of the main gas band and soot radiation in each of the flames, based on the position of these peaks in the mean spectra at this height. At each wavelength point the range in radiation intensity, from zero to the maximum recorded at that point, was divided into ten equally spaced "bins." The first "bin" covering the region from 0 to 10% of the maximum and the second from 10 to 20%, continuing up to the tenth "bin" covering the region from 90 to 100% of the maximum. The data from the "single-shot" spectra were then sorted into these "bins," giving the relative frequencies for the intensity variations. The data were normalized by dividing each relative frequency by the total number of "single-shot" spectra. This yielded a discrete representation of the probability density function (PDF) of radiation intensity at each of these wavelength points.

RESULTS AND DISCUSSION

Given the central position occupied by mixture fraction in conserved scalar modelling of the gaseous species in the fast chemistry limit and that of temperature in respect of finite rate chemistry and radiative heat transfer, the accu-

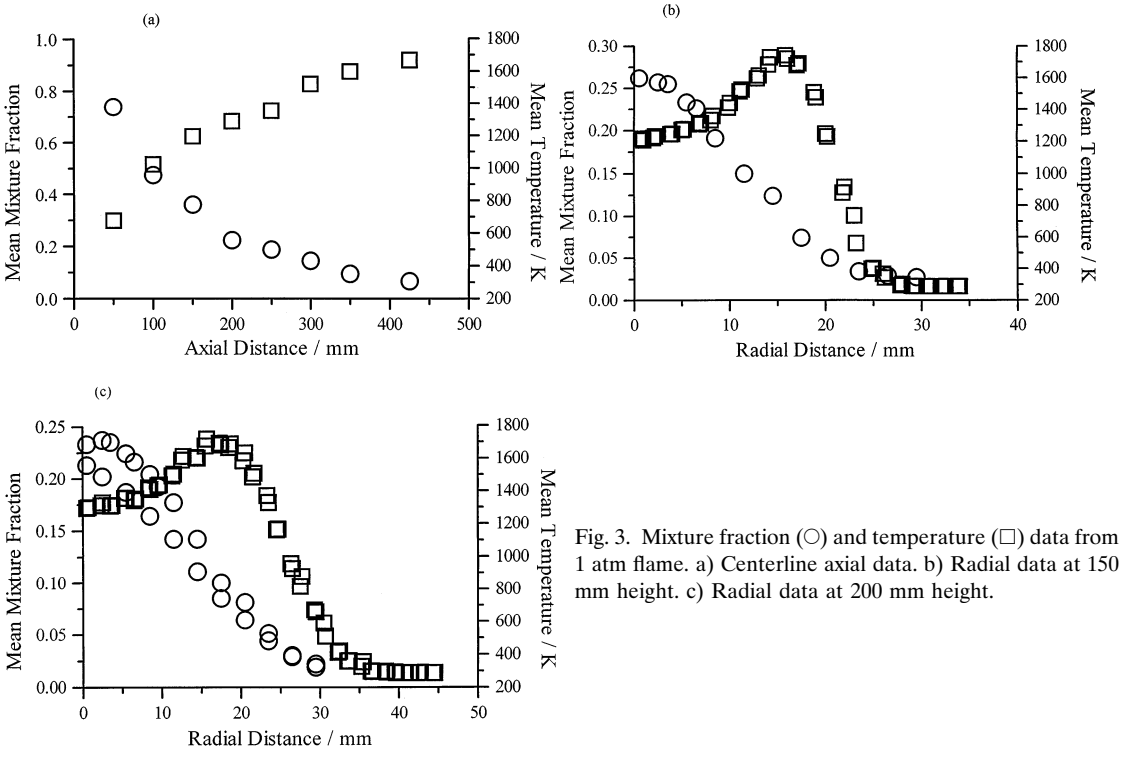

Fig. 3. Mixture fraction (○) and temperature (□) data from 1 atm flame. a) Centerline axial data. b) Radial data at 150 mm height. c) Radial data at 200 mm height.

rate prediction of these properties features prominently in model development and validation. The measured distributions of mean mixture fraction and temperature, both axial and radial, in the atmospheric pressure flame (Flame 1) are summarised in Figs. 3–5. Radial profiles are presented at discrete flame heights of 150, 200, 250, 300, 350, and 425 mm. As discussed earlier, the centerline value of mixture fraction at the 150 mm height, inferred from the measured CO_2/N_2 ratio, is significantly lower (see Fig. 3b) than that shown in Fig. 3a, determined using the argon tracer technique. The data from complete traverses of the flame have been folded about the jet centreline, demonstrating their underlying symmetry. The peak mean temperature is observed to decline gradually with increasing flame height and to migrate towards the centreline under the combined influences of turbulent transport and enhanced radiative loss.

Despite having the same mass flowrate, the 3 atm flame (Flame 2) is revealed in Figs. 6a–d to be substantially shorter than its atmospheric pressure counterpart, as evidenced by the peak

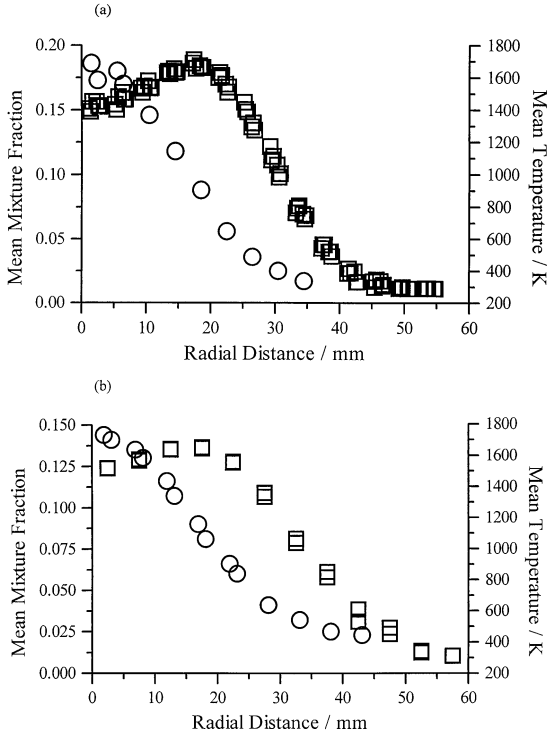

Fig. 4. Mixture fraction (○) and temperature (□) data from 1 atm flame (a) Radial data at 250 mm height. (b) Radial data at 300 mm height.

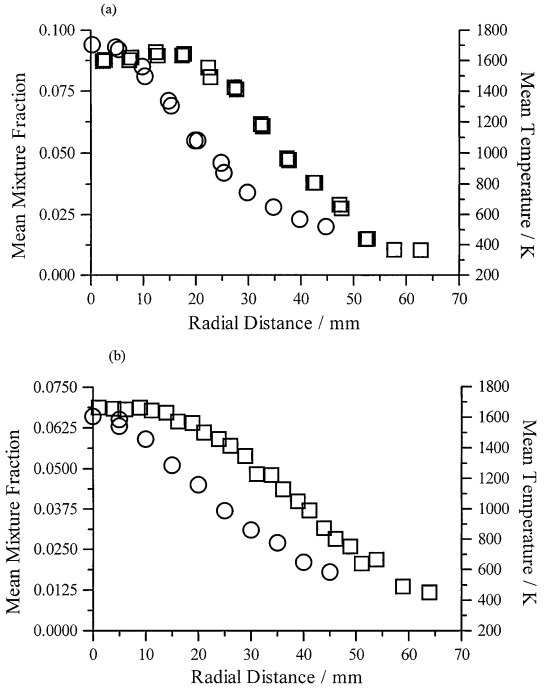

Fig. 5. Mixture fraction (○) and temperature ([]) data from 1 atm flame (a) Radial data at 350 mm height. (b) Radial data at 425 mm height.

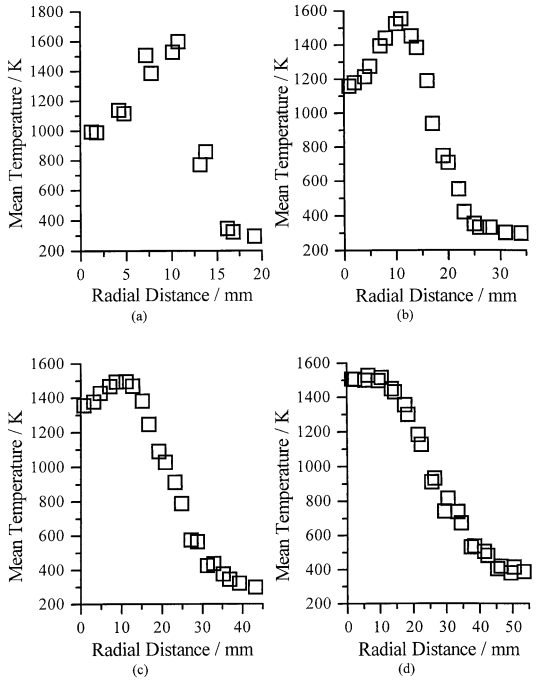

Fig. 6. Radial temperature data from 3 atm flame. a) 100 mm height. b) 150 mm height. c) 200 mm height. d) 250 mm height.

temperature reaching the flame centreline earlier. The density difference between hot and cold gas is greater in the 3 atm flame. Hence, buoyancy induced acceleration is more important at the high pressure. This increased flame acceleration will create more turbulence, enhancing the fuel and air mixing, and shortening the flame. The peak temperatures are also generally lower in Flame 2, consistent with the increased radiative heat loss from the flame due to the higher soot loading. The temperature distributions also indicate that the radial spread of the higher pressure flame is less than that of Flame 1. Mixture fraction measurements were not undertaken in this flame.

The evolution with flame height of the radial profiles of soot volume fraction are presented in Figs. 7 and 8. The low levels of soot in Flame 1 restrict the data to the regions of maximum production, at heights of 300 mm and above. The peak values (~0.2 ppm) are comparable with the levels measured in laminar methane diffusion flames [3]. The measurements at 3 atm provide a more comprehensive picture of the growth with flame height and subsequent decay under the influence of oxidation and dilution mixing. The peak values here approach an order of magnitude increase over those observed at atmospheric pressure, a substantially greater apparent sensitivity to pressure than observed in the jet flames of more heavily sooting, prevaporised kerosene by Young et al. [21], where a broadly linear variation is described. As might be expected, given the intermittent nature of soot production and the restricted nature of

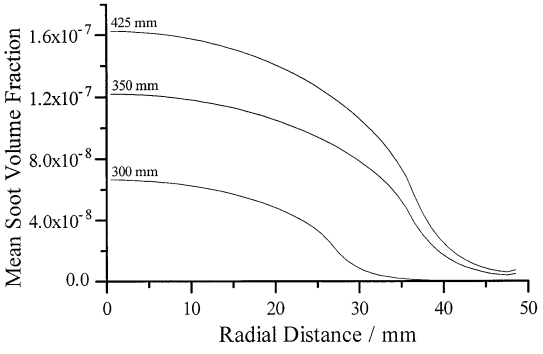

Fig. 7. Radial soot volume fraction profiles from 1 atm flame. Profile heights as indicated on the figure.

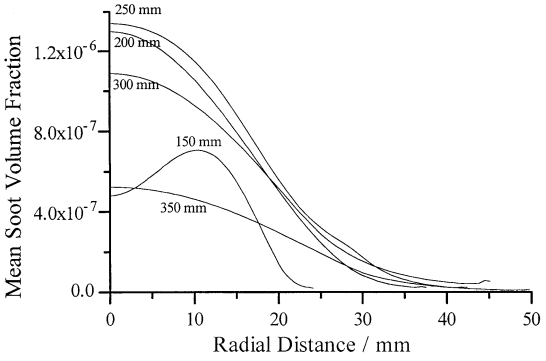

Fig. 8. Radial soot volume fraction profiles from 3 atm flame. Profile heights as indicated on the figure.

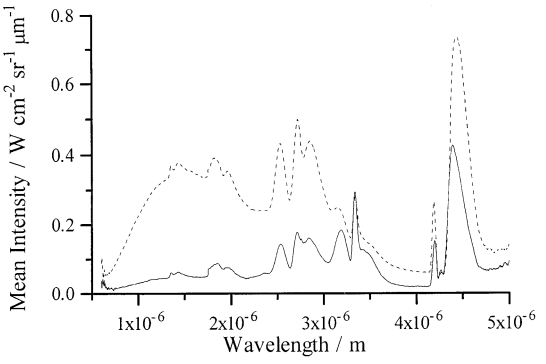

Fig. 10. Radiation emission spectra from 3 atm flame. Solid line (—) from 100 mm height, dotted line (—) from 250 mm height.

particle diffusive transport, the radial spread of the mean soot profiles is significantly less than for other scalars such as temperature (cf. Figs. 4 and 6).

The impact of soot growth on the radiation from Flame 1 is clearly shown in Fig. 9. At 150 mm height the mean radiation intensity, along a line of sight, is dominated by the banded emission from gaseous CO_2 and H_2O. The broadband contribution from soot is revealed at the 425 mm height. This same trend is displayed more dramatically by Flame 2 (cf. Fig. 10). In particular the spectrum from the 250 mm position exhibits a very large contribution from the continuum radiation of the soot. A significant increase in the magnitude of the banded emission from the gases accompanying the downstream flame spread is also noted.

While those turbulent flame predictions that do include radiative exchange, in general, employ models incorporating the local time-averaged properties (composition and temperature), there is concern over the impact of turbulent scalar fluctuations and the underlying multi-point spatial correlations on the radiation intensity, both in practice and from a modelling standpoint [22]. Figures 11a–d and 12a–d show the statistical distributions of intensity at specific wavelengths in the two flames, recorded at the 250 mm height. While the distributions at the wavelength dominated by carbon dioxide emissions (~4.3 μm) show a comparatively limited spread in intensity (Figs. 11d, 12d), those at shorter wavelengths, which typically incorporate more of the soot continuum, exhibit wider variation and some intermittency (Figs. 11a–c 12a–c). A fourfold variation in intensity is not untypical. Substantially larger variations are to be anticipated in more heavily buoyant fires [23].

The presentation of data here is intended to provide a comprehensive description of these flames for model evaluation purposes. Some additional data have been excluded on the grounds of space, however, and these are fully reported in Brookes [24].

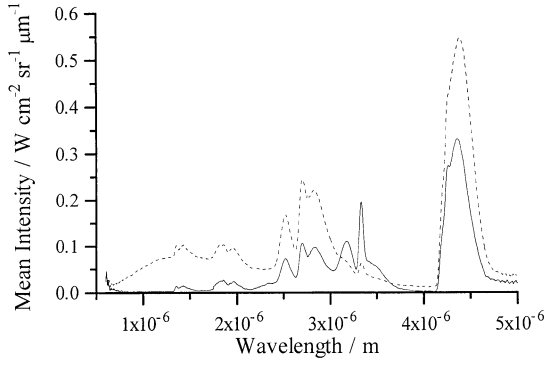

Fig. 9. Radiation emission spectra from 1 atm flame. Solid line (—) from 150 mm height, dotted line (—) from 425 mm height.

CONCLUSIONS

The development of computational models of coupled soot formation and radiation heat transfer is presently limited by the paucity of data on their joint behaviour in turbulent nonpremixed flames. Comprehensive property maps of mean mixture fraction, temperature,

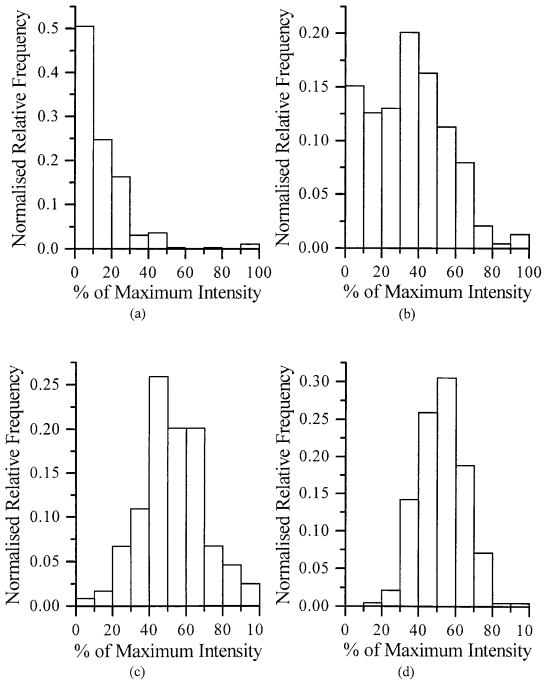

Fig. 11. Discrete PDFs of radiation intensity at the 250 mm height from 1 atm flame. a) λ = 1650 nm, maximum intensity = 0.153 W cm^{-2} sr^{-1} μm^{-1}. b) λ = 2834 nm, maximum intensity = 0.468 W cm^{-2} sr^{-1} μm^{-1}. c) λ = 3332 nm, maximum intensity = 0.320 W cm^{-2} sr^{-1} μm^{-1}. d) λ = 4359 nm, maximum intensity = 0.907 W cm^{-2} sr^{-1} μm^{-1}.

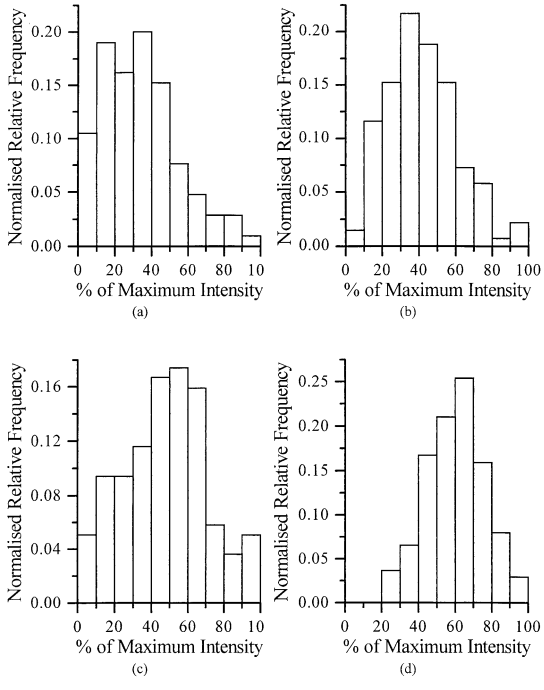

Fig. 12. Discrete PDFs of radiation intensity at 250 mm height from 3 atm flame. a) λ = 1700 nm, maximum intensity = 0.985 W cm^{-2} sr^{-1} μm^{-1}. b) λ = 2846 nm, maximum intensity = 1.045 W cm^{-2} sr^{-1} μm^{-1}. c) λ = 3342 nm, maximum intensity = 0.587 W cm^{-2} sr^{-1} μm^{-1}. d) λ = 4435 nm, maximum intensity = 1.220 W cm^{-2} sr^{-1} μm^{-1}.

soot volume fraction, and radiation intensity, properties critical to such model development, are reported in two confined methane jet flames, burning at pressures of 1 and 3 atm. The measurements at the higher pressure permit the models to be assessed over a wider range of operating conditions, while also introducing enhanced levels of soot production and radiative flux which facilitate measurement.

The three-fold increase in operating pressure produces increases in soot volume fraction approaching an order of magnitude, shifting the balance of contributions to the radiative flux from the gaseous species, principally CO_2 and H_2O, to soot. This pressure dependence is larger than has been observed in similar confined flame studies employing more heavily sooting fuels, such as pre-vaporized kerosine.

At the higher pressure, the jet flame may be considered to mimic the behaviour of a much larger methane release, but at a scale which is accessible to detailed diagnostic measurement.

The statistical distributions of radiation intensity, inferred from the measurements with the rotating grating monochromator, indicate large (approximately fourfold) intensity variations from the fluctuating soot continuum. This effect is also more pronounced at the higher pressure.

The authors are pleased to acknowledge the support and interest of BG plc and the Engineering and Physical Sciences Research Council in this research.

REFERENCES

1. Faeth, G. M., Jeng, S.-M., and Gore, J. P., *Heat Transfer in Fire and Combustion Systems*, HTD Vol. 45, ASME, (1985) pp. 137–151.
2. Kent, J. H., and Honnery, D., *Combust. Sci. Tech*. 54:383–397 (1987).
3. Syed, K. J., Stewart, C. D., and Moss, J. B., *Twenty-Third Symposium (International) on Combustion*, The Combustion Institute, 1990, pp. 1533–1541.
4. Fairweather, M., Jones, W. P., Ledin, H. S., and Lindstedt, R. P., *Twenty-Fourth Symposium (Interna-*

tional) on Combustion, The Combustion Institute, 1992, pp. 1067–1074.
5. Hassan, M. M. A., Lockwood, F. C., and Moneib, H. A., Fluctuating Temperature and Mean Concentration Measurements in a Vertical Turbulent Free Jet Diffusion Flame, *Italian Flame Days*, International Flame Research Foundation, 1980.
6. Jeng, S.-M., Lai, M.-C., and Faeth, G. M., *Combust. Sci. Tech*. 40:41–53 (1984).
7. Young, K. J., *Soot Formation in Turbulent Vaporised Kerosine-Air Jet Flames at Elevated Pressure*, Ph.D. thesis, Cranfield University, 1993, England.
8. Fristrom, R. M., and Westenberg, A. A., *Flame Structure*, McGraw-Hill, New York, 1965.
9. Hughey, B. J., and Santavicca, D. A., *Combust. Sci. Tech*. 29:167–190 (1982).
10. Shepp, L. A., and Logan, B. F., *IEEE Trans. Nuclear Science* 21:21–30 (1974).
11. Kerker, M., *The Scattering of Light*, Academic Press, London, 1969.
12. Mullins, J., and Williams, A., *Fuel* 66:277–280 (1987).
13. Moss, J. B., Stewart, C. D., and Syed, K. J., *Twenty-Second Symposium (International) on Combustion*, The Combustion Institute, 1988, pp. 413–423.
14. Garo, A., *Mechanismes de Formation et de Destruction des Particles de Carbone dans une Flamme de Diffusion Laminaire Methane-Air*, Ph.D. thesis, Universite de Haute-Alsace, 1984, France.
15. Dalzell, W. H., and Sarofim, A. F., *J. Heat Transfer* 91:100–104 (1969).
16. Lee, S. C., and Tien, C. L., *Eighteenth Symp. (International) on Combustion*, The Combustion Institute, 1981, pp. 1159–1166.
17. Chippet, S., and Gray, W. A., *Combust. Flame* 31:149–159 (1978).
18. Selamet, A., and Arpaci, V. S., *Combust. Sci. Tech*. 78:165–175 (1991).
19. Megaridis, C. M., and Dobbins, R. A., *Twenty-Second Symposium (International) on Combustion*, The Combustion Institute, 1988, pp. 353–362.
20. Kumar, S., and Tien, C. L., *Combust. Sci. Tech*. 66: 199–216 (1989).
21. Young, K. J., Stewart, C. D., and Moss, J. B., *Twenty-Fifth Symposium (International) on Combustion*, The Combustion Institute, 1994, pp. 609–617.
22. Gore, J. P., and Faeth, G. M., *Twenty-First Symposium (International) on Combustion*, The Combustion Institute, 1986, pp. 609–617.
23. Sivathanu, Y. R., Kounalakis, M. E., and Faeth G. M., *Twenty-Third Symposium (International) on Combustion*, The Combustion Institute, 1990, pp. 1543–1550.
24. Brookes, S. J., *Soot Production and Thermal Radiation from Turbulent Jet Diffusion Flames*, Ph.D. thesis, Cranfield University, 1996, England.

Received 1 May 1997; revised 10 February 1998; accepted 12 February 1998